

PROCEEDINGS OF SPIE

SPIDigitalLibrary.org/conference-proceedings-of-spie

Dental composites for wide color matching

Humbel, Mattia, Mattle, Corinne, Scheel, Mario, Diaz, Ana, Jerjen, Iwan, et al.

Mattia Humbel, Corinne Mattle, Mario Scheel, Ana Diaz, Iwan Jerjen, Robert Lominski, Robert Sterchi, Georg Schulz, Andres Izquierdo, Guido Sigron, Hans Deyhle, Bert Müller, "Dental composites for wide color matching," Proc. SPIE 12041, Bioinspiration, Biomimetics, and Bioreplication XII, 1204102 (20 April 2022); doi: 10.1117/12.2613110

SPIE.

Event: SPIE Smart Structures + Nondestructive Evaluation, 2022, Long Beach, California, United States

Dental Composites for Wide Color Matching

Mattia Humbel^a, Corinne Carlucci^a, Mario Scheel^b, Ana Diaz^c, Iwan Jerjen^d, Robert Lominski^e, Robert Sterchi^f, Georg Schulz^a, Andres Izquierdo^a, Guido Sigron^a, Hans Deyhle^g, and Bert Müller^a

^aBiomaterials Science Center, University of Basel, Allschwil, Switzerland

^bBeamline Anatomix, Synchrotron SOLEIL, Gif-sur-Yvette, France

^cPaul Scherrer Institute, Villigen, Switzerland

^dGloor Instruments, Kloten, Switzerland

^ePerkinElmer, Schwerzenbach, Switzerland

^fInstitute of Materials and Process Engineering, Zürcher Hochschule für angewandte Wissenschaften, Winterthur, Switzerland

^gDiamond Light Source, Didcot, United Kingdom

ABSTRACT

Dental fillings are selected according to the color of the patient's tooth. Therefore, the dentists have around a dozen colors for each product in stock. Still, after a certain period of time, the choice could become suboptimal as the hard tooth tissue alters, for example, owing to specific habits such as smoking. Nanotechnology-based composites can at least partially master this deficiency. Similar to a chameleon, a filling with such a composite can match the color of the surrounding enamel. In this study, we thoroughly investigated the nanostructure of one such composite and the related optical properties. The size of the spherical silica-zirconia fillers and their arrangement in micrometer-sized domains was examined using electron microscopy, synchrotron radiation-based nanotomography and small-angle X-ray scattering. The optical properties were derived from transmission measurements ranging from the ultraviolet to the infrared spectrum. Isotropic dielectric homogenization was used to model the optical properties based on the nanostructure. We could deduce the diameter of the spheres, which corresponds to 260 nm. The spheres show a narrow size distribution and form micrometer-sized domains with close-packed nanospheres along their borders. Homogenization was not sufficient to predict all features of the transmission spectrum. The gathered structural information is a basis to gain deeper understanding of the chameleon effect and the methodology can be applied to other single-shade dental composites.

Keywords: Dental filling, composite shades, structural color, chameleon effect, biomimetics, nanotomography, small-angle X-ray scattering, spectrophotometry

1. INTRODUCTION

Caries is one of the most widespread diseases worldwide, affecting billions of patients.¹ Therefore advances in restorative dentistry have a significant impact. In the past decades, tooth fillings were often made of metal alloys such as amalgam. In the last 25 years, these metals have increasingly been replaced by dental resin composites consisting of ceramic filler particles embedded in a polymer matrix.² The filling material is applied in viscous form and then cured with ultraviolet light to become solid, typically with a halogen-like broadband spectrum from 385 to 515 nm. This procedure is convenient for the practising dentist and the resulting restorations show mechanical properties similar to those of the abovementioned metallic filling materials.

In order to get an esthetically pleasing result, the dental composites are coloured with pigments in a set of shades. The dentist tries to find the shade that matches the patient's tooth color. This process takes time and the results are all too often imperfect, as there generally is a limited number of shades available, the appearance

Further author information: (Send correspondence to M.H.)

M.H.: E-mail: humbemat@student.ethz.ch, Telephone: +41 76 499 70 77

B.M.: E-mail: bert.mueller@unibas.ch, Telephone: +41 61 207 54 30

Bioinspiration, Biomimetics, and Bioreplication XII, edited by Raúl J. Martín-Palma
Mato Knez, Akhlesh Lakhtakia, Proc. of SPIE Vol. 12041, 1204102
© 2022 SPIE · 0277-786X · doi: 10.1117/12.2613110

of the filling may change when wet, and so on. Dental composites of all shades needs to be kept in stock. More importantly, tooth colour may change with age, depending on the habits of the patient like drinking coffee or smoking. In that case, the dental filling that once would have blended in with the tooth can later stand out due to a mismatch in hue. Therefore it is desirable to have a single dental filling material available which fits the appearance of the tooth, regardless of the tooth's shade and age.

A number of companies now offer such single-shade dental resin composites. The restorations are said to exhibit the chameleon effect, meaning that the light emitted from the restoration surface has a similar optical spectrum as that coming from the tooth's surface. A perceived blending of color between tooth and restoration had been shown for multi-shade composites before,³ and found to be not only perceptual.⁴ A comparison between a single-shade composite and two pigmented ones demonstrated a stronger chameleon effect in the former.⁵ In the same study, a contribution of structural color to the chameleon effect was suggested.

Structural color is a widespread phenomenon in nature,⁶ observed for example in precious opals⁷ and the feathers of birds such as the magpie.⁸ In contrast to ordinary color, where the appearance of a material is based on selective absorption of light at certain wavelengths, structural color arises due to constructive interference of light scattered at structures on a length scale comparable to the wavelength. For example, the rapid color changes in the skin of panther chameleons, see Fig. 1, are achieved by tuning a lattice of guanine nanocrystals.⁹

In this study we investigate how the size and spatial distribution of filler particles with diameters on the submicron scale contribute to the optical properties of dental composites, especially with respect to the chameleon effect mentioned above.

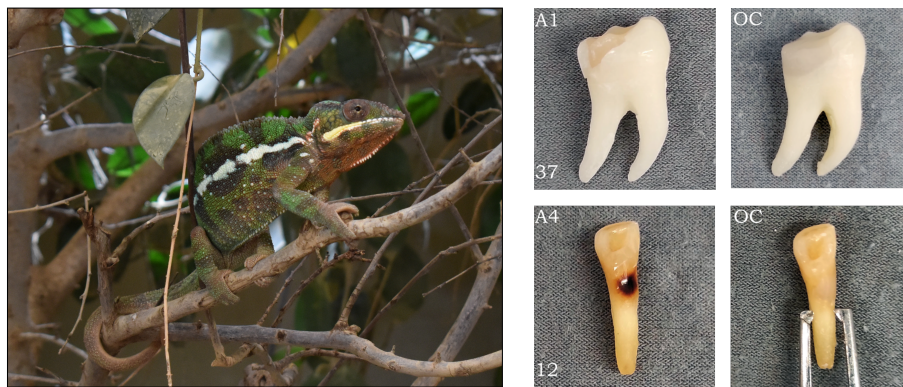


Figure 1. Left: The panther chameleon (*furcifer pardalis*) blends into its surroundings. Its ability to rapidly change color is based on a tunable lattice of nanocrystals producing structural color.⁹ Right: Composite nanosphere dental restorations attempt to match the color of the surrounding tooth, cp. the same tooth before and after restorations in the second and third columns, respectively. For large restorations, especially at the edge of the crown, the chameleon effect is unsatisfactory, see the top row. The color is well matched for small restorations, see bottom row.¹⁰

2. MATERIALS AND METHODS

2.1 Sample preparation

Cylindrical samples of the omnichroma dental composite (Tokuyama Dental, Tokyo, Japan) with a target diameter of 100 μm and a length of around 10 mm were fabricated by rolling the material out to the desired shape and UV cured with a Bluephase G4 curing light (Ivoclar Vivadent, Schaan, Liechtenstein). Disks with a target thickness of 100 μm and a radius of around 10 mm were fabricated by pressing portions of the material between blocks of acrylic glass. For diameter estimation, the cylindrical samples were imaged from the side in a scanning electron microscope (EM-30AXN, Coxem Daejeon, Korea) and with microtomography in a Skyscan 1275 system (Bruker, Karlsruhe, Germany). The diameter was measured at three heights near the tip and averaged.

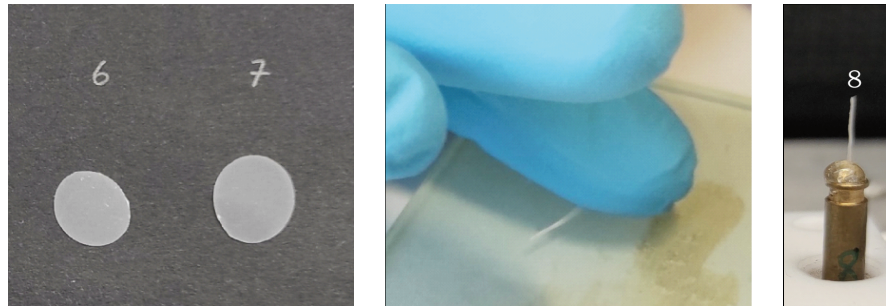


Figure 2. Left: Two of the disk-like samples for optical transmission measurements. Center: Preparation of a cylindrical sample for nanotomography and X-ray scattering experiments. Right: A cylindrical sample glued onto a brass sample holder for the acquisition of the projections for tomographic imaging.

2.2 Imaging by electron microscopy

The fracture surface of an omnichroma cylinder was imaged with an EM-30AXN scanning electron microscope (Coxem, Daejeon, Korea) at an acceleration voltage of 15 keV.

2.3 Transmission measurements and data interpretation

The transmission of light with wavelengths ranging from 190 nm to 2500 nm through a disk of omnichroma was measured in intervals of 5 nm with a Lambda 1500+ spectrophotometer (PerkinElmer, Waltham MA, USA) with integrating sphere.

In an electromagnetic homogenization approach, the effective permittivity of a material consisting of silica spheres with a radius of 130 nm occupying a volume fraction of 68 % within a UDMA matrix was determined for wavelengths between 200 nm and 800 nm. The refractive index of UDMA was assumed to be 1.484 independent of wavelength.¹¹ For silica, the refractive index at arbitrary wavelengths was determined by interpolation based on results compiled by Philipp.¹² The isotropic-dielectric specialization of the Bruggemann equation was solved numerically to obtain the effective permittivity ϵ_{Br} of the homogenized composite material, see equation (6.9) in Mackay and Lakhtakia.¹³ The transmittance was then determined by solving the transfer matrix equation for a homogeneous dielectric layer of 100 μm thickness and permittivity ϵ_{Br} .

2.4 Small-angle X-ray scattering experiments

Synchrotron small-angle X-ray scattering (SAXS) measurements were performed at the cSAXS beamline at the Swiss Light Source, Paul Scherrer Institute, Switzerland. X-rays with a photon energy of 11.2 keV were focused at the sample, where the beam had a size of 28 μm \times 8 μm (horizontal \times vertical). SAXS data were collected from a position in the middle of the sample using a Pilatus 2M detector placed at a distance of about 7 m from the sample. An evacuated flight tube was placed in between the sample and the detector to reduce air absorption and scattering. We performed 50 acquisitions of 0.25 s each and averaged them. A background subtraction was performed with a similar measurement without sample.

Small-angle X-ray scattering measurements were also performed with a Nanostar laboratory system (Bruker, Karlsruhe, Germany). A sticky hard sphere model with logarithmic-normal size distribution was fitted to the synchrotron SAXS data using the SASfit software (version 0.94.11).¹⁴

2.5 Transmission X-ray microscopy for tomographic imaging

Nanotomography measurements were performed with the full-field transmission X-ray microscope at the Anatomix beamline, synchrotron SOLEIL, France.¹⁵ Local tomograms of the cylindrical samples were acquired at a photon energy of 10 keV, with isotropic pixels of 17.4 nm size.

A 45 \times 370 \times 370 pixel subvolume of a tomogram was selected. Within this subvolume, the centers of the spherical filler particles were determined by applying a Jerman blob enhancement filter,¹⁶ thresholding at a “blobness” value of 0.01 and extracting the centers of labeled regions with scikit-image.¹⁷

3. RESULTS

3.1 Sample preparation

The needle-like samples for nanotomography and related X-ray scattering experiments had cylindrical or conical shape, with the diameter near the tip ranging from 50 μm to 190 μm , as shown in Fig. 3.

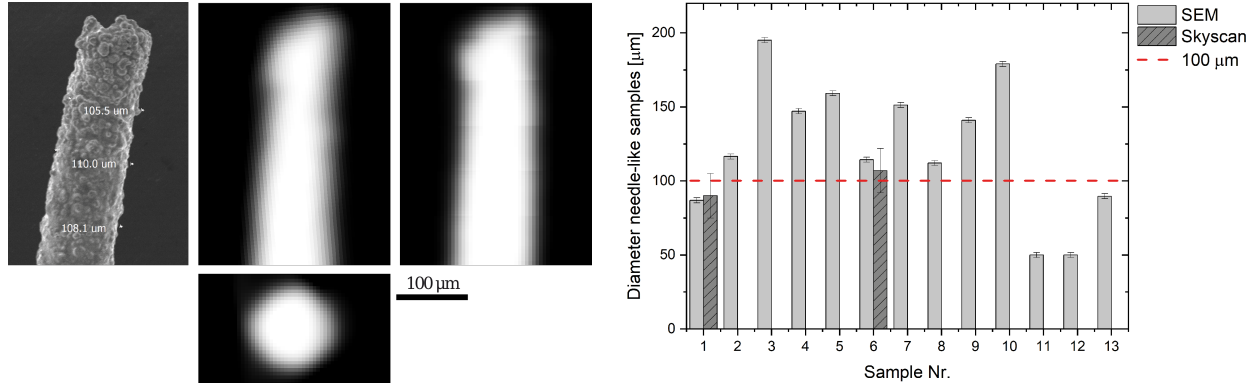


Figure 3. Left: Electron micrograph and orthogonal slices through the tip of a needle-like sample used for diameter estimation. Right: The sample diameters measured near the tip. The dashed line shows the desired diameter of 100 μm for nanotomography.

3.2 Imaging by electron microscopy

The scanning electron microscopy images show that the surfaces of the omnichroma samples feature spherical domains with diameters of a few micrometers where the silica/zirconia nanospheres are almost close-packed, see Fig. 4. Between these domains the filler particles seem to be less ordered. Deviations from the spherical shape can hardly be seen, the particles appear to have a narrow size distribution.

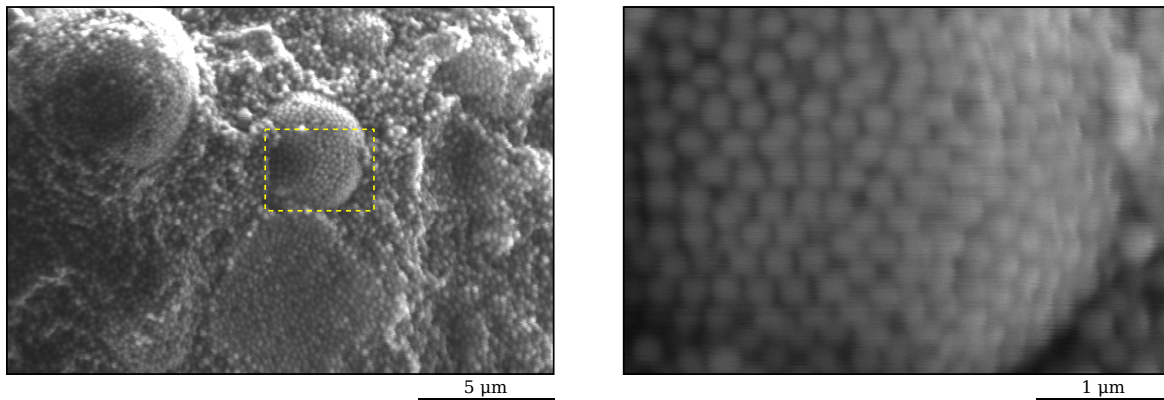


Figure 4. Left: Electron micrograph of a fractured composite surface, which shows domains of ordered submicron filler particles of spherical shape. The rectangle indicates the location of the micrograph acquired with higher magnification, given on the right.

3.3 Transmission X-ray microscopy for tomographic imaging

The microdomains observed with electron microscopy are not only present at the sample surface, but throughout its volume, as the tomograms acquired by transmission X-ray microscopy show, see Fig. 5. However, their shape is not perfectly spherical, they instead form ellipsoid-like volumes, see Fig. 5 on the right. Furthermore, the tight

packing of spheres is observed mainly at the domain borders, while the filler density is less inside the domains. From the sphere centers that were extracted from the TXM data, a mean distance to the nearest neighbor of (183.2 ± 0.9) nm was computed, with a standard deviation of (39.5 ± 0.9) nm. The distribution shown in Fig. 6 has an enhanced tail on the side of longer distances, around 260 nm.

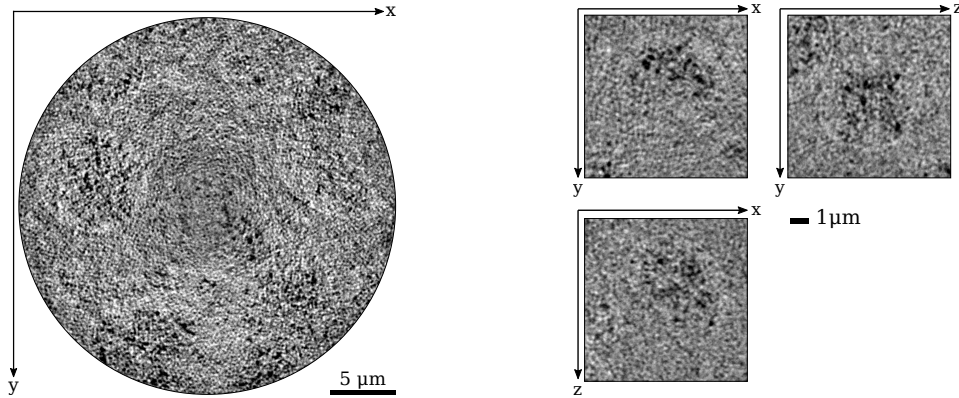


Figure 5. Left: Slice through a tomogram of a cylindrical sample, featuring spherical micrometer-sized domains. Right: Orthogonal slices showing one of the micrometer-sized domains, for a video see <http://dx.doi.org/10.1117/12.2613110>

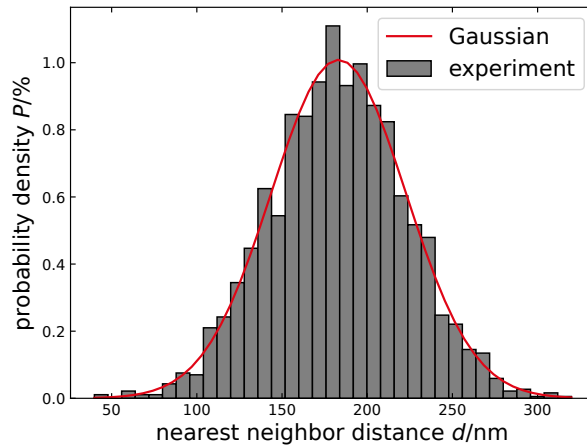


Figure 6. Distribution of the distance to the nearest neighbor for the centers of mass of the spherical filler particles. The red line is a Gaussian distribution with a mean of 183 nm and a standard deviation of 40 nm.

3.4 Small-angle X-ray scattering experiments

The small-angle X-ray scattering data from both the synchrotron and the laboratory measurement are shown after angular integration in Fig. 7, together with the transmission X-ray microscopy data after a discrete Fourier transform. A curve fit for a sticky hard sphere model with a logarithmic-normal size distribution to the synchrotron SAXS data, also shown in Fig. 7, gives a mean radius of 130 nm. The hard-sphere radius was 116 nm and the corresponding volume fraction was 42.8%. With the laboratory SAXS setup, intensity values for wave numbers below 0.1 nm^{-1} were damped by the presence of the beam stop and therefore not considered. Above this limit, the data largely agrees with the synchrotron SAXS measurement. The Fourier transformed TXM data shows a similar fall-off behavior as the SAXS measurements at large wave numbers. The oscillations in the synchrotron SAXS data are echoed in the TXM data by bends at $2.6 \times 10^{-2} \text{ nm}^{-1}$, $4.7 \times 10^{-2} \text{ nm}^{-1}$, and $5.9 \times 10^{-2} \text{ nm}^{-1}$. For wave numbers below $2.5 \times 10^{-2} \text{ nm}^{-1}$, the intensity in the TXM data keeps rising and does not show the plateau that the synchrotron SAXS data exhibits.

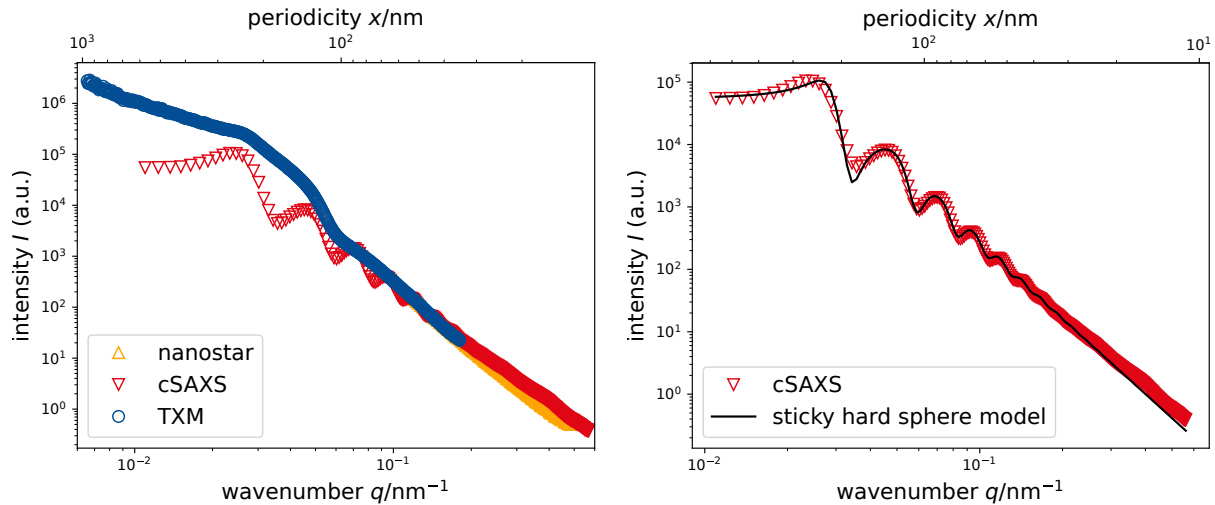


Figure 7. Left: Small angle x-ray scattering (SAXS) measured at the cSAXS beamline at the Swiss Light Source (red) and with a nanostar laboratory setup (orange). In blue the values obtained by a discrete Fourier transform on the 3D transmission x-ray microscopy data from the Anatomix beamline at SOLEIL. Right: Curve fit for a sticky hard sphere model to the cSAXS data.

3.5 Transmission measurements and data interpretation

The optical transmittance of a disk of omnichroma for wavelengths ranging from 190 nm to 2500 nm, measured with a spectrophotometer with integrating sphere, is shown in Fig. 8. The material is mostly transparent in the visible and near-infrared range, with a transmittance between 74.9% and 91.7%. There is a drop in the IR-B range at 2200 nm to values between 65% and 75%. For ultraviolet light, the transmittance drops significantly, from 74.9% at 400 nm to 3.1% at 350 nm. A peak in the transmittance could be observed centered at 263.5 nm, the full width at half maximum being 20.0 nm.

The transmittance was modeled by isotropic dielectric homogenization. The homogenization approach resulted in an overestimation of the absorption in the visible range. Also, it predicted a peak in the ultraviolet, centered at 315 nm, that could not be observed experimentally. The position of this peak changes neither when varying the radius of the filler particles, nor when varying the thickness of the sample in the model. The much smaller peak that does occur in the experimental data, is on the other hand absent from the computed transmittance. Where model and experiment agree is that the transmittance in the visible range increases with wavelength and that far enough into the ultraviolet range, everything is absorbed.

4. DISCUSSION

4.1 Imaging by electron microscopy

Electron microscopy of the fracture surface of a cylindrical sample of the omnichroma dental composite has shown micrometer-sized spherical domains of tightly packed filler. A clustering of filler particles has been observed before for the 3M Filtek Universal composite, where the sub-100 nm particles form clusters of around 1 μm to 3 μm in size.^{18,19} The resonant scattering of light from inhomogeneities with no long-ranged order resulting in angle-independent structural color is determined by the mean spacing between neighboring sites,²⁰ therefore the presence of domains with a smaller average spacing is expected to influence the optical properties of the whole restoration.

4.2 Transmission X-ray microscopy for tomographic imaging

Nanotomography confirmed the presence of micrometer-sized domains throughout the sample volume, but showed that a tight packing of spheres occurs mainly at the domain borders. The distance between neighboring particles follows a normal distribution centered at 183 nm. Given that small-angle X-ray scattering suggests a narrowly

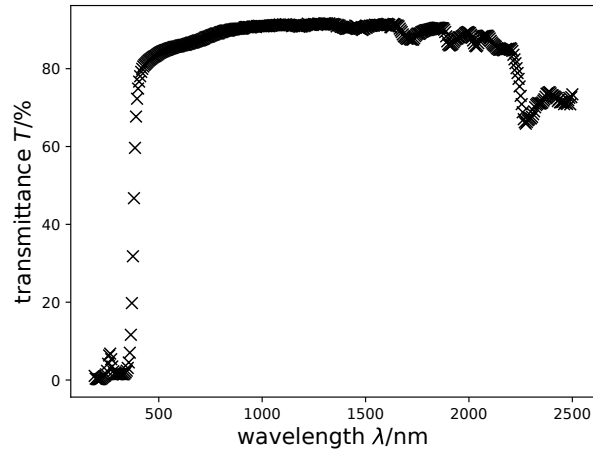


Figure 8. Spectral transmittance of a disk-like sample of the dental composite. The sample is transparent in the visible and infrared range and opaque in the ultraviolet range, except for a noticeable peak centered at 260 nm, the diameter of the filler spheres.

distributed particle radius of 130 nm, this indicates an overlap between the filler particles. However, at least at the fracture surface examined by electron microscopy, such an overlap or deformation of the submicron spheres cannot be observed.

4.3 Small-angle X-ray scattering experiments

The parameter estimation for a sticky hard sphere model on the synchrotron SAXS data for the omnichroma dental composite indicated a narrow distribution of particle radii centered at 130 nm. This is in agreement with the uniform diameter of 260 nm indicated by the manufacturer.²¹ To the extent that the surface sensitivity of electron microscopy allows, this estimate is also consistent with the electron micrographs. The estimated radius of the sticky hard spheres in the structure factor differs from the already mentioned sphere radius in the form factor by 11 %. However, while there is good agreement overall, the position of the structure factor peak predicted by the model differs from the one observed experimentally by around 20 nm, suggesting that this discrepancy stems from the model incompletely reflecting the structure.

4.4 Transmission measurements and data interpretation

The theoretical estimation of the transmittance by a homogenization approach for a simplified model of the dental composite showed significant differences to the experimentally measured transmittance. Homogenization assumes the constituent particles of a composite to be small compared to the wavelength of light in the material.¹³ However, as the filler particles have diameters of 260 nm and a wavelength of 800 nm in vacuum corresponds to 540 nm in silica, the refractive index at that wavelength being 1.46, this assumption is not fulfilled here for visible and ultraviolet light. Therefore at most qualitative results can be expected here. Magkiriadou *et al.* have used a single-scattering model to calculate the reflection from colloidal glasses of 170, 240, and 330 nm PMMA particles, where they were able to qualitatively predict the reflection, including the position of peaks due to structural color.²⁰ Hwang *et al.* modeled polystyrene nanoparticles with radii of 94, 109, and 138 nm using a Monte Carlo simulation for multiple scattering and could quantitatively predict the reflectance.²²

5. CONCLUSION

We have gathered extensive information on the mesoscopic structure of one particular single-shade dental composite relevant for the understanding of the chameleon effect. The methods employed here can be applied to other single-shade composite materials in the future, to examine how composition, size and shape of the filler particles influence the chameleon effect. More information can be extracted from the already gathered data,

for instance on spatial variations in the interparticle distance. It can also serve as the basis for more sophisticated simulations. Structural color is a relevant topic of current research and more biomimetic applications of structural color can be expected in the near future.

ACKNOWLEDGMENTS

We thank Griffin Rodgers, Christine Tanner, Melissa Osterwalder, Jeannette von Jackowski, and Thomas Pfohl for their support. ANATOMIX is an Equipment of Excellence (EQUIPEX) funded by the *Investments for the Future* program of the French National Research Agency (ANR), project *NanoimagesX*, grant no. ANR-11-EQPX-0031.

REFERENCES

- [1] Kassebaum, N., Smith, A., Bernabé, E., Fleming, T., Reynolds, A., Vos, T., Murray, C., Marcenes, W., and GBD 2015 Oral Health Collaborators, “Global, regional, and national prevalence, incidence, and disability-adjusted life years for oral conditions for 195 countries, 1990–2015: A systematic analysis for the global burden of diseases, injuries, and risk factors,” *Journal of Dental Research* **96**(4), 380–387 (2017). PMID: 28792274.
- [2] Cho, K., Rajan, G., Farrar, P., Prentice, L., and Prusty, B. G., “Dental resin composites: A review on materials to product realizations,” *Composites Part B: Engineering* **230**, 109495 (2022).
- [3] Paravina, R. D., Westland, S., Imai, F. H., Kimura, M., and Powers, J. M., “Evaluation of blending effect of composites related to restoration size,” *Dental Materials* **22**(4), 299–307 (2006).
- [4] Tsubone, M., Nakajima, M., Hosaka, K., Foxton, R. M., and Tagami, J., “Color shifting at the border of resin composite restorations in human tooth cavity,” *Dental Materials* **28**(8), 811–817 (2012).
- [5] Kobayashi, S., Nakajima, M., Furusawa, K., Tichy, A., Hosaka, K., and Tagami, J., “Color adjustment potential of single-shade resin composite to various-shade human teeth: Effect of structural color phenomenon,” *Dental Materials Journal* **40**(4), 1033–1040 (2021).
- [6] Vukusic, P. and Sambles, J. R., “Photonic structures in biology,” *Nature* **424**(6950), 852–855 (2003).
- [7] Sanders, J. V., “Colour of precious opal,” *Nature* **204**(4964), 1151–1153 (1964).
- [8] Pol Vigneron, J., Colomer, J.-F. m. c., Rassart, M., Ingram, A. L., and Lousse, V., “Structural origin of the colored reflections from the black-billed magpie feathers,” *Phys. Rev. E* **73**, 021914 (Feb 2006).
- [9] Teyssier, J., Saenko, S. V., van der Marel, D., and Milinkovitch, M. C., “Photonic crystals cause active colour change in chameleons,” *Nature Communications* **6**(1), 6368 (2015).
- [10] Mattle, C., *Nanostructural characterization of a dental filling for wide color matching*, Master’s thesis, University of Basel (2021).
- [11] Watson Noke Scientific, “Urethane dimethacrylate(UDMA) CAS 72869-86-4.” <https://www.watsonnoke.com/urethane-dimethacrylateudma-cas-72869-86-4>. Accessed 22 February 2022.
- [12] Philipp, H., “Silicon dioxide (SiO₂) (glass),” in [*Handbook of Optical Constants of Solids*], Palik, E. D., ed., 749–763, Academic Press, Burlington (1997).
- [13] Mackay, T. G. and Lakhtakia, A., [*Modern Analytical Electromagnetic Homogenization with Mathematica® (Second Edition)*], 2053-2563, IOP Publishing (2020).
- [14] Breßler, I., Kohlbrecher, J., and Thünemann, A. F., “SASfit: a tool for small-angle scattering data analysis using a library of analytical expressions,” *Journal of Applied Crystallography* **48**, 1587–1598 (Oct. 2015). Number: 5 Publisher: International Union of Crystallography.
- [15] Weitkamp, T., Scheel, M., Giorgetta, J. L., Joyet, V., Roux, V. L., Cauchon, G., Moreno, T., Polack, F., Thompson, A., and Samama, J. P., “The tomography beamline ANATOMIX at synchrotron SOLEIL,” *Journal of Physics: Conference Series* **849**, 012037 (June 2017). Publisher: IOP Publishing.
- [16] Jerman, T., Pernuš, F., Likar, B., and Špiclin, Ž., “Blob Enhancement and Visualization for Improved Intracranial Aneurysm Detection,” *IEEE Transactions on Visualization and Computer Graphics* **22**, 1705–1717 (June 2016). Conference Name: IEEE Transactions on Visualization and Computer Graphics.
- [17] Walt, S. v. d., Schönberger, J. L., Nunez-Iglesias, J., Boulogne, F., Warner, J. D., Yager, N., Goullart, E., and Yu, T., “scikit-image: image processing in Python,” *PeerJ* **2**, e453 (June 2014). Publisher: PeerJ Inc.

- [18] Durand, L. B., Ruiz-López, J., Perez, B. G., Ionescu, A. M., Carrillo-Pérez, F., Ghinea, R., and Pérez, M. M., “Color, lightness, chroma, hue, and translucency adjustment potential of resin composites using ciede2000 color difference formula,” *Journal of Esthetic and Restorative Dentistry* **33**(6), 836–843 (2021).
- [19] 3M Oral Care, “3M Filtek universal restorative,” tech. rep., 3M Deutschland GmbH (2019).
- [20] Magkiriadou, S., Park, J.-G., Kim, Y.-S., and Manoharan, V. N., “Absence of red structural color in photonic glasses, bird feathers, and certain beetles,” *Phys. Rev. E* **90**, 062302 (Dec 2014).
- [21] Tokuyama Dental, “Omnichroma,” tech. rep., Tokuyama Dental (2019).
- [22] Hwang, V., Stephenson, A. B., Barkley, S., Brandt, S., Xiao, M., Aizenberg, J., and Manoharan, V. N., “Designing angle-independent structural colors using Monte Carlo simulations of multiple scattering,” *Proceedings of the National Academy of Sciences* **118**(4) (2021).